Nonreciprocal wave transmission through an extended discrete nonlinear Schrödinger dimer

Muhammad Abdul Wasay*
Department of Physics, University of Agriculture, Faisalabad 38040, Pakistan;
Center for Theoretical Physics of Complex Systems, Institute for Basic Science (IBS), Daejeon 34051, Republic of Korea;
and National Centre for Physics, Quaid-i-Azam University Campus, Islamabad, Pakistan
(Received 12 July 2017; revised manuscript received 7 October 2017; published 21 November 2017)

We analyze a one-dimensional extended discrete nonlinear Schrödinger (DNLS) dimer model for nonreciprocal wave transmission. The extension corresponds to the addition of a nonlocal or intersite nonlinear response in addition to a purely cubic local (on-site) nonlinear response, which refines the purely cubic model and aligns to more realistic situations. We observe that a diodelike action persists in the extended case; however, the inclusion of nonlocal response tends to reduce the diode action. We show that this extension results in achieving the diode effect at lower incoming intensities as compared to the purely cubic case. We also report that a nearly perfect diode action is possible in the extended case for a higher level of asymmetry between on-site potentials than its cubic counterpart. Moreover, we vary different site-dependent parameters to probe for regimes of a better diode effect within this extended model. We also present the corresponding stability analysis for the exact stationary solutions to the extended DNLS equation, we discuss the bifurcation behavior in detail, and we explicitly give the regions of stability.

DOI: 10.1103/PhysRevE.96.052218

I. INTRODUCTION

Symmetry breaking usually brings about novel physical phenomena, which can sometimes be very useful for making certain devices. Recently, much attention has been paid toward the search for devices that can control energy or mass flow. A diode is one such device. It can control transport, be it electric current or in the context of acoustics [1–3], heat flow [4–6], or electromagnetic (EM) waves [7–10]. With regard to waves, a nonreciprocal or asymmetric transmission is the basic ingredient to design a wave diode. In a linear and time-reversal symmetric system, asymmetric propagation (of waves) is not allowed by the reciprocity theorem [11–13]. One can, however, break the time-reversal symmetry by the application of a magnetic field to achieve the desired effect, which also has an acoustic analog [14].

However, in a nonlinear system such a phenomenon can be brought about in an entirely different manner, and it seems more appealing as it is possible in a nonlinear system to achieve propagation control without having to apply any external field for breaking the system's symmetry. In fact, asymmetric propagation can be caused by the nonlinear properties of the material itself. The basic underlying phenomenon is that parity symmetry is broken by the nonlinear medium itself. The first such phenomenon was reported in [15], where the author observed a nonreciprocal transmission of phonons through a nonlinear layer in between two different crystals. It has been explored much in the nonlinear optics realm. For instance, in [16,17] a so called all-optical diode was proposed.

There have been several relevant studies concerning the wave diode proposal. In [18–20], for example, the authors proposed a wave diode for a nonlinear system. The system was comprised of a one-dimensional nonlinear lattice that was modeled by a purely cubic discrete nonlinear Schrödinger (DNLS) equation. A specific number of lattice sites having nonlinearity were embedded inside an infinite linear lattice. A non-Kerr law or saturable nonlinearity analog of the above with two nonlinear sites (dimer) was investigated for asymmetric propagation in [21], and nonreciprocal transmission through nonlinear $\mathcal{PT}$-symmetric oligomers was studied in [22].

In this work, we will study asymmetric wave propagation through a one-dimensional "extended" nonlinear dimer that is connected to linear side chains. We will use the DNLS equation to model the system, as it is fully integrable for dimers (much like the earlier models), and it is one of the simplest dynamical lattice models to be analyzed theoretically. The DNLS model has become popular in studying nonlinear optics problems. For example, a DNLS equation can be used to model the distribution of light solitons in AlGaAs waveguide arrays [23]. However, as compared to some earlier works mentioned above, our model is significantly different in that we will use an "extended" DNLS equation to model our system. The "extension" corresponds to a nonlocal or intersite nonlinearity. A quantum analog of this model was studied in the context of fast energy transfer for a nonlinear quantum lattice in [24] and for the vibrational dynamics of a nonlinear quantum dimer coupled to a phonon bath in [25].

We will include an intersite or nonlocal nonlinearity, and with the inclusion of this nonlocal response the system establishes a cooperative (local and nonlocal) nonlinear response. We will examine how the nonreciprocal transmission is effected under this cooperation by varying the strength of nonlocal response and different site-dependent parameters.

The physical motivation to study such a system lies in the idea that, as before, the nonlinear dimer is embedded into a linear lattice, but now the medium between the two sites (dimer) is also nonlinear. This will strengthen the nonlocal nonlinear effect, and incoming waves will experience a cooperative (local+nonlocal) nonlinear response from the lattice. This is the motivation for the current work on the extended model. This physical situation is more realistic as it takes into account more effects. Moreover, the question of whether asymmetric propagation of incoming waves persists in physical situations in which there is such a cooperative nonlinear response, and to what extent this physical model

*wasay31@gmail.com

can exhibit a diodelike action, is still open, and the purpose of this paper is to address that question. Following [26], we will also analyze the stability of exact stationary solutions to the asymmetric (different on-site potentials) extended DNLS dimer and the corresponding bifurcation behavior in the presence of this new intersite nonlinearity.

The paper is organized as follows: In Sec. II, we introduce the extended DNLS model, establish the transmission formulas, and plot the corresponding results. In Sec. III, we supply the exact stationary solutions and develop three corresponding cases (symmetric, antisymmetric, and soliton). In Sec. IV, the stability analysis of these solutions is carried out. In Sec. V, we present the corresponding bifurcation behavior. Section VI contains a summary and conclusion.

II. MODEL AND FORMALISM

We will use a set of discrete nonlinear Schrödinger equations to model our system. These time-dependent DNLS equations with a nonlocal nonlinearity are

$$i\frac{dA_n}{dt} = V_nA_n - \gamma_n|A_n|^2A_n - \epsilon_0(A_{n+1}+A_{n-1}) - \epsilon_n(|A_{n+1}|^2A_n + |A_{n-1}|^2A_n). \quad (1)$$

This set of dynamical equations is obtained from a Hamiltonian that is a classical version of the vibron Hamiltonian in a quantum lattice with attractive Hubbard type interaction between bosons, described in Refs. [24,25],

$$H = \sum_n \left[V_n|A_n|^2 - \frac{\gamma_n}{2}|A_n|^4 - \epsilon_n(A_{n+1}^*A_n^*A_{n+1}A_n) - \epsilon_0(A_n^*A_{n+1} + A_{n+1}^*A_n)\right]. \quad (2)$$

The dynamical set of equations in (1) have stationary solutions of the form $A(t) = \phi e^{-i\omega t}$. Using these in Eq. (1), one arrives at

$$\omega\phi_n = V_n\phi_n - \phi_{n+1} - \phi_{n-1} + \gamma_n|\phi_n|^2\phi_n + \epsilon_n(|\phi_{n+1}|^2\phi_n + |\phi_{n-1}|^2\phi_n), \quad (3)$$

where ω is the spatial frequency, ϕ_n is the complex amplitude at site n with potential V_n, and ϵ_n is the nonlocal nonlinearity. We further assume that γ_n, ϵ_n, and V_n are nonvanishing only for $1 \leqslant j \leqslant N$, where j represents nonlinearity at a particular site and N represents the total number of nonlinear sites ($N = 2$ for dimer). This setup assumes the dimer to be at site 1 and site 2 in a large one-dimensional lattice, therefore j runs from 1 to 2 and n runs over the whole lattice. This will allow free propagation outside the nonlinear region. We consider plane-wave solutions of the form

$$\phi_n = \begin{pmatrix} Ie^{iKn} + Re^{-iKn} & n \leqslant 1 \\ Te^{iKn} & n \geqslant N \end{pmatrix}, \quad (4)$$

where I, R, and T represent the amplitude of the incident, reflected, and transmitted wave, respectively. K is the wave number. From (4), the amplitude at the interface of the nonlinear dimer (for waves with $K > 0$) is $\phi_2 = Te^{i2K}$ and $\phi_3 = Te^{i3K}$. We are interested in examining the transmission properties of these plane waves. For the (linear) region $n > N$, we have

$$\omega Te^{iKn} = -Te^{iK(n+1)} - Te^{iK(n-1)} \Rightarrow \omega = -2\cos(K). \quad (5)$$

The spatial frequency is $\omega = -2\cos(K)$ and $0 \leqslant K \leqslant \pi$ for the wave impinging the lattice from the left. Note that (4) is a solution to Eq. (3) for $n \neq j$ only when K satisfies Eq. (5). The lattice is still mirror-symmetric with respect to the center of the nonlinear region. To achieve the desired diode effect by breaking the lattice's mirror symmetry, we must supplement the system with a translational asymmetry together with the already present nonlinearities [18,27]. We must therefore choose one of the three parameters such that either $V_j \neq V_{N-j+1}$ or $\gamma_j \neq \gamma_{N-j+1}$ or $\epsilon_j \neq \epsilon_{N-j+1}$. The transmission coefficient for right-moving waves is obtained by flipping the lattice [18,19]. The encountered sites are now relabeled as $1 \to N', 2 \to (N-1)', \ldots, N \to 1$ so that to solve for the transmission coefficient with $K < 0$, one simply needs to replace $V_j = V_{N-j+1}$, i.e., to replace V_1 by V_2 and so on. Here $K < 0$ is used to denote a negative wave number associated with a right-moving wave.

For $n = 0$, we have

$$\phi_0 = I + R$$

and for $n = 1$,

$$\phi_1 = Ie^{iK} + Re^{-iK}.$$

With ϕ_0 and ϕ_1, the reflected and incident amplitudes are

$$R = \frac{\phi_0e^{iK} - \phi_1}{e^{iK} - e^{-iK}} \quad (6)$$

and

$$I = \frac{\phi_0e^{-iK} - \phi_1}{e^{-iK} - e^{iK}}. \quad (7)$$

A standard approach to determine the transmission coefficient [$t(K,|T|^2) = \frac{|T|^2}{|I|^2}$] is to use the backward iterative map [28–30]. From (3), we get

$$\phi_{n-1} = -\phi_{n+1} + (V_n - \omega + \gamma_n|\phi_n|^2)\phi_n + \epsilon_n(|\phi_{n+1}|^2 + |\phi_{n-1}|^2)\phi_n. \quad (8)$$

A. Extended DNLS dimer and its bistable behavior

Let us now focus on our case of interest, i.e., the dimer (two nonlinear sites). From (8) with $n = 2$, we have

$$\phi_1 = Te^{2iK}(\delta_2 - e^{iK}),$$

where $\delta_2 = (V_2 - \omega + \gamma_2|T|^2 + \epsilon_2|T|^2)$.

For $n = 1$,

$$\phi_0 = Te^{2iK}[\delta_1(\delta_2 - e^{iK}) - 1]$$

with $\delta_1 = V_1 - \omega + \gamma_1|T|^2|(\delta_2 - e^{iK})|^2 + \epsilon_1|T|^2$.

From (7),

$$|I|^2 = \frac{|T|^2|(\delta_2 - e^{iK})(\delta_1 - e^{iK}) - 1|^2}{|e^{-iK} - e^{iK}|^2}$$

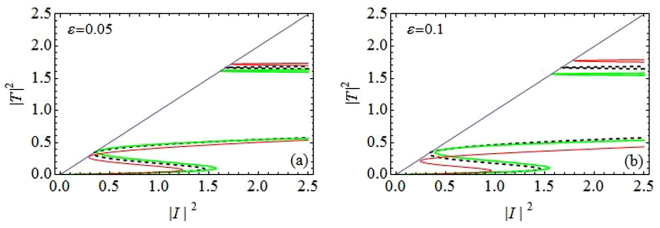

FIG. 1. $|T|^2$ as a function of $|I|^2$. Extended DNLS dimer with (a) $\varepsilon = 0.05$ and (b) $\varepsilon = 0.1$; ε denotes asymmetry in the on-site potential.

and

$$|T|^2 = \frac{|I|^2|e^{-iK} - e^{iK}|^2}{|(\delta_2 - e^{iK})(\delta_1 - e^{iK}) - 1|^2}.$$

So, the transmission coefficient is

$$t(K,|T|^2) = \left|\frac{e^{-iK} - e^{iK}}{(\delta_2 - e^{iK})(\delta_1 - e^{iK}) - 1}\right|^2. \quad (9)$$

Now let us define

$$\zeta_2 = V_1 - \omega + \gamma_1|T'|^2 + \epsilon_1|T'|^2,$$

$$\zeta_1 = V_2 - \omega + \gamma_2|T'|^2|(\zeta_2 - e^{iK'})|^2 + \epsilon_2|T'|^2.$$

By doing the same procedure of a backward iterative map, one obtains for the right-moving wave with $K' = -K$

$$|I'|^2 = \frac{|T'|^2|(\zeta_2 - e^{iK'})(\zeta_1 - e^{iK'}) - 1|^2}{|e^{-iK'} - e^{iK'}|^2},$$

$$|T'|^2 = \frac{|I'|^2|e^{-iK'} - e^{iK'}|^2}{|(\zeta_2 - e^{iK'})(\zeta_1 - e^{iK'}) - 1|^2}$$

$$\Rightarrow t'(K',|T'|^2) = \left|\frac{e^{-iK'} - e^{iK'}}{(\zeta_2 - e^{iK'})(\zeta_1 - e^{iK'}) - 1}\right|^2. \quad (10)$$

To introduce the required asymmetry, we assume a different on-site potential $V_j = V_0(1 \pm \varepsilon)$ for the two nonlinear sites (dimer), the two nonlinear sites are equivalent in nonlinearity with $V_0(1+\varepsilon)$ at site 1 and $V_0(1-\varepsilon)$ at site 2, ε is the extent of asymmetry, and V_0 is the depth of the potential. The solutions are determined by iterating (8) from $\phi_N = T\exp(iKN)$, $\phi_{N+1} = T\exp[iK(N+1)]$. One must note that for the periodic point of the map, i.e., $(\phi_0,\phi_1) = (\phi_N,\phi_{N+1})$, the transmission is maximal with $t = 1$.

Figure 1 corresponds to the extended DNLS dimer case. It gives a relationship between incident intensity ($|I|^2$ along the horizontal axis) and transmitted intensity ($|T|^2$ along the vertical axis) with $V_0 = -2.5$, $\gamma_{1,2} = 1$, $\epsilon_{1,2} = 0.50$, and $K = 0.1$. Figure 1(a) is produced with $\varepsilon = 0.05$ and Fig. 1(b) is for $\varepsilon = 0.1$. The dashed black line corresponds to the symmetric branch. The green line corresponds to left-moving waves with $K > 0$, and the red line corresponds to right-moving waves with $K < 0$. Due to asymmetry ε, the two waves with $K < 0$ and $K > 0$ have a pronounced difference in transmission, leading to the asymmetric transmission. In Fig. 1(b), we increase the asymmetry in the on-site potentials and observe a broader window (bistability window) for perfect transmission. In contrast to [18,19], we observe that refining the DNLS model by adding a nonlocal nonlinearity results in achieving the diode effect at lower incoming intensities, at the cost of a reduction in the window of complete transmission.

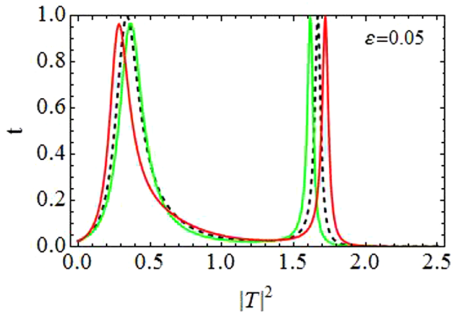

FIG. 2. Transmission coefficient t as a function of transmitted intensity $|T|^2$: Extended DNLS dimer.

We further observe that the intervals (bistability windows) of maximal transmission shrink by increasing the strength of the nonlocal nonlinearity ϵ. For very small values of ϵ (e.g., for a value of 0.20), the diode interval broadens and approaches the purely cubic DNLS results [18], as expected.

Figure 2 is a plot for transmission coefficient t as a function of transmitted intensity. It is produced for $\varepsilon = 0.05$ and $\epsilon = 0.5$; other parameters are as before.

B. Results

We introduce a rectifying factor following [18], which determines the regions with maximum diode effect, however it does not address the magnitude of the transmission coefficient. It is given by

$$f = \frac{t(K,|T|^2) - t(-K,|T|^2)}{t(K,|T|^2) + t(-K,|T|^2)}. \quad (11)$$

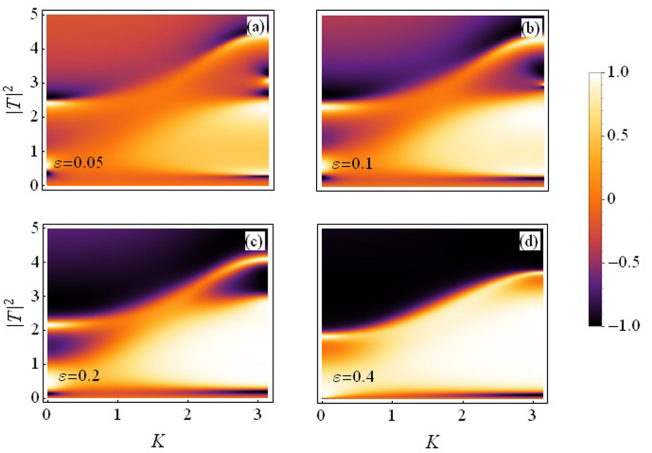

FIG. 3. Rectifying factor as a function of $|T|^2$ and K for a purely (on-site) cubic DNLS dimer: For distinct and increasing asymmetry between on-site potentials.

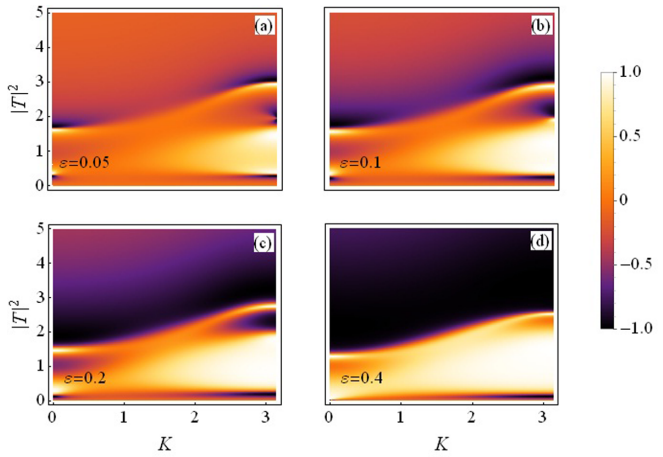

FIG. 4. Rectifying factor as a function of $|T|^2$ and K for an extended DNLS dimer: For distinct and increasing asymmetry between on-site potentials.

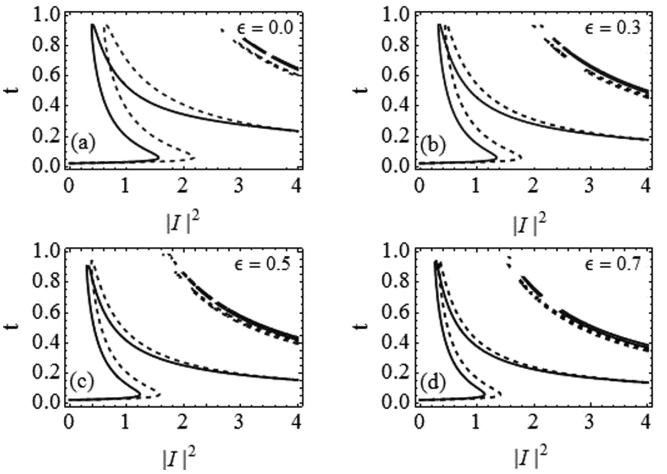

FIG. 6. Transmission coefficient t as a function of incident wave intensity $|I|^2$ for distinct (increasing) values of nonlocal nonlinear response ϵ.

The following plots are produced for the rectifying factor with varying asymmetry. The yellow regions indicate transmission of right-moving waves ($K < 0$) only, and the black regions indicate transmission of left-moving waves ($K > 0$) only.

In Figs. 3 and 4, we have plotted the rectifying factor as a function of transmitted intensity $|T|^2$ and K. Figure 3 is a reproduction from [18]. The purpose of reproducing it is to make a comparison with Fig. 4, which is the rectifying factor plot for the extended DNLS dimer case. This will allow one to understand how this cooperative local and nonlocal nonlinear response from the lattice affects the diode features produced by nonreciprocal transmission. Note that Fig. 3 is for a purely cubic DNLS dimer, which means that there is only one on-site cubic nonlinear response from the lattice.

For fixed γ and ϵ, increasing asymmetry results in an improvement in the diode action, which can be seen in both figures. However, as mentioned above, the overall transmission shrinks in the extended case due to an increased nonlinear response that an incoming wave experiences from the lattice. Furthermore, note that in Fig. 3(d), one can observe that a nearly perfect diode action occurs for the purely cubic case with $\varepsilon = 0.4$ and also that the right-moving waves have a slightly higher contribution to the diode action as compared to the left-moving waves. For the extended case with $\varepsilon = 0.4$ in Fig. 4(d), there is a small region corresponding to small wave numbers that does not exhibit a perfect diode action; however, for the region with perfect diode action, the contribution of the right- and left-moving waves is roughly the same.

The extended DNLS dimer shows an almost perfect diode behavior for an increased asymmetry between on-site potentials at $\varepsilon = 0.7$, as compared to its purely cubic counterpart where this phenomenon is achieved at $\varepsilon = 0.4$, and the contribution to this diode action from the left-moving waves is higher as compared to the right-moving waves. This is depicted in Fig. 5.

All plots in Fig. 6 are produced for a fixed value of asymmetry, $\varepsilon = 0.05$. The plot in Fig. 6(a) is for the purely cubic case with no nonlocal response; the window of maximum transmission is visible. Subsequent plots Figs. 6(b)–6(d) are produced for increasing nonlocal nonlinear response, and we

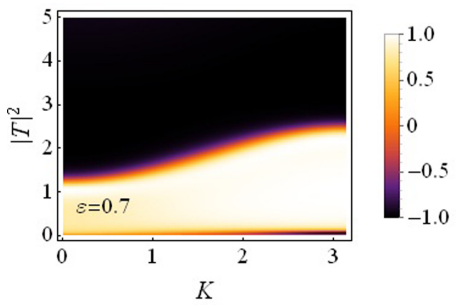

FIG. 5. Rectifying factor as a function of $|T|^2$ and K, extended DNLS dimer: For asymmetry between on-site potentials set to $\varepsilon = 0.7$.

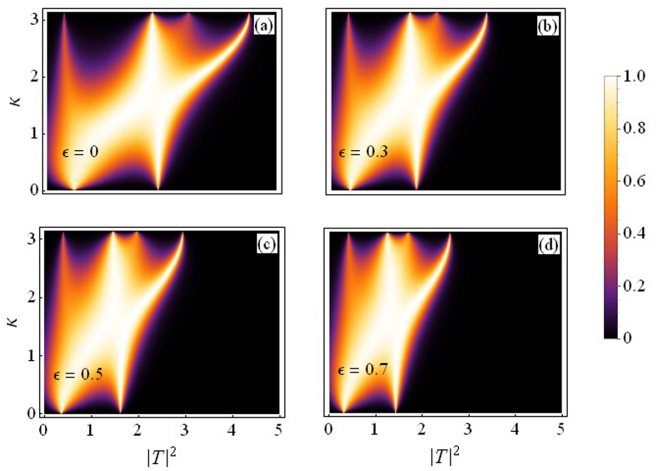

FIG. 7. Transmission coefficient as a function of $|T|^2$ and K: For increasing nonlocal nonlinear response ϵ in (a)–(d) and fixed asymmetry $\varepsilon = 0.05$.

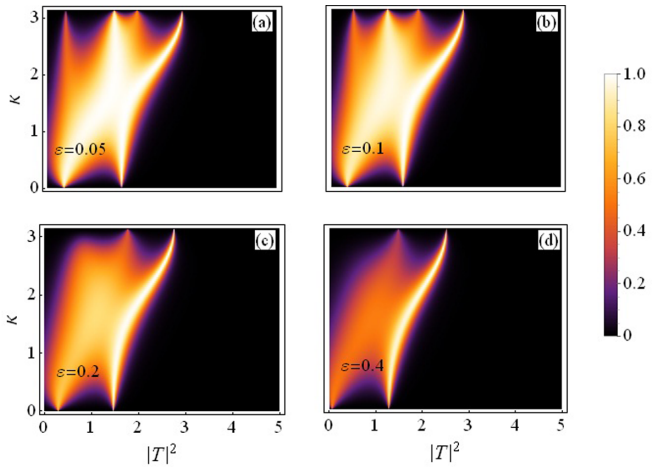

FIG. 8. Transmission coefficient as a function of $|T|^2$ and K: For increasing asymmetry ε in (a)–(d) and fixed nonlocal nonlinear response $\epsilon = 0.5$.

have strengthened the nonlocal nonlinearity from $\epsilon = 0.3$ in Fig. 6(b) to $\epsilon = 0.7$ in Fig. 6(d). One can clearly see that the window shrinks but is displaced to lower input intensities with increasing nonlocal nonlinear response.

Figures 7 and 8 represent the plots for the transmission coefficient as a function of $|T|^2$ and K for $0 \leqslant K \leqslant \pi$. The asymmetry is fixed at $\varepsilon = 0.05$ in Fig. 7. The plot in Fig. 7(a) is for the purely cubic case. We then turn on the nonlocal response and plot for different strengths of this nonlocal nonlinear response [$\epsilon = 0.3$ in Fig. 7(b) to $\epsilon = 0.7$ in Fig. 7(d)]. One can see a shrinking transmission pattern as this nonlocal term gets strengthened. Figure 8 is the same plot, but here we fix the intersite strength to $\epsilon = 0.5$ and vary the asymmetry. It is interesting to note that in the top (horizontal) panel corresponding to Figs. 8(a) and 8(b), the transmission peaks split from two to four roughly around $K = \frac{\pi}{2}$ for asymmetry values up to $\varepsilon = 0.1$, while this peak-splitting pattern tends to diminish as we increase the asymmetry. Also note that the transmission of incoming waves with larger wave numbers ($K > \frac{\pi}{2}$) and waves with smaller wave numbers ($K < \frac{\pi}{2}$) is approximately the same.

III. STATIONARY SOLUTIONS

A dimer has two degrees of freedom, and the corresponding two conserved quantities render it a fully integrable system. For a system with two sites, $n = 2$, the dynamical equation

$$\frac{\partial H}{\partial A_n^*} = \frac{\partial A_n}{\partial t}, \tag{12}$$

with H defined by Eq. (2), leads to two coupled equations with a different on-site potential,

$$i\frac{dA_1}{dt} = V_1 A_1 - \gamma_1 |A_1|^2 A_1 - \epsilon_0 A_2 - \epsilon_1 |A_2|^2 A_1, \tag{13}$$

$$i\frac{dA_2}{dt} = V_2 A_2 - \gamma_1 |A_2|^2 A_2 - \epsilon_0 A_1 - \epsilon_1 |A_1|^2 A_2. \tag{14}$$

γ_1 is the on-site (cubic) nonlinearity and ϵ_1 is the nonlocal (intersite) nonlinearity, as before. The norm (number) is given by

$$N = |A_n|^2. \tag{15}$$

The stationary solutions are solutions of the form $A_1 = \phi_1 e^{-i\omega t}$ and $A_2 = \phi_2 e^{-i\omega t}$; ϕ_i is time-independent. Using these in (13) and (14) leads to a set of three equations,

$$\omega = V_1 - \gamma |\phi_1|^2 - \epsilon_0 \frac{\phi_2}{\phi_1} - \epsilon_1 |\phi_2|^2, \tag{16}$$

$$\omega = V_2 - \gamma |\phi_2|^2 - \epsilon_0 \frac{\phi_1}{\phi_2} - \epsilon_1 |\phi_1|^2, \tag{17}$$

$$N = |\phi_1|^2 + |\phi_2|^2. \tag{18}$$

A subtraction between (16) and (17) leads to

$$\left((\gamma - \epsilon_1) - \frac{\epsilon_0}{\phi_1 \phi_2} + \frac{(V_1 - V_2)}{(\phi_2^2 - \phi_1^2)}\right)(\phi_2^2 - \phi_1^2) = 0. \tag{19}$$

Equation (19) together with the definition of N gives three different solutions.

A. Symmetric solution

The symmetric solution is

$$\phi_1 = \sqrt{\frac{N}{2}} \quad \text{and} \quad \phi_2 = \sqrt{\frac{N}{2}}$$

with the corresponding equations

$$\omega_{\uparrow\uparrow} = V_1 - \epsilon_0 - \frac{N}{2}(\gamma + \epsilon_1)$$

and

$$\omega_{\uparrow\uparrow} = V_2 - \epsilon_0 - \frac{N}{2}(\gamma + \epsilon_1).$$

B. Antisymmetric solution

The antisymmetric solution is

$$\phi_1 = \sqrt{\frac{N}{2}} \quad \text{and} \quad \phi_2 = -\sqrt{\frac{N}{2}}$$

with the corresponding equations

$$\omega_{\uparrow\downarrow} = \epsilon_0 - \frac{N}{2}(\gamma + \epsilon_1) + V_1$$

and

$$\omega_{\uparrow\downarrow} = \epsilon_0 - \frac{N}{2}(\gamma + \epsilon_1) + V_2.$$

C. Soliton solution

The soliton solution turns out to be slightly different. After some computation, we get the soliton solution from Eq. (19) in the following form:

$$\phi_1 = \sqrt{\frac{N}{2}\left(1 + \sqrt{1 - \frac{2\epsilon_0^2 - (V_1 - V_2)^2}{N^2(\gamma - \epsilon_1)^2}}\right)} \tag{20}$$

and

$$\phi_2 = \sqrt{\frac{N}{2}\left(1 - \sqrt{1 - \frac{2\epsilon_0^2 - (V_1 - V_2)^2}{N^2(\gamma - \epsilon_1)^2}}\right)} \tag{21}$$

with the corresponding equations

$$\omega_{\uparrow}. = V_1 - \gamma N \quad \text{and} \quad \omega_{\uparrow}. = V_2 - \epsilon_1 N.$$

Please also note that we have obtained the soliton solutions (20) and (21) in the limit $(\gamma - \epsilon_1) \gg \epsilon_0$.

D. Interpretation

The symmetric and antisymmetric solutions simply represent the solution for the coupled oscillator. But we should explain the soliton solution as it appears to be quite different. It exists for $\gamma > \frac{2(V_1-\omega-\epsilon_0)}{N} - \epsilon_1$, which accounts for the strength of on-site nonlinearity for the soliton solution, and $\epsilon_1 > \frac{2(V_2-\omega-\epsilon_0)}{N} - \gamma$ and $\epsilon_1 > \frac{2(V_2-\omega+\epsilon_0)}{N} - \gamma$, which account for the strength of nonlocal nonlinearity. Note that by increasing the nonlinearity such that $(\gamma - \epsilon_1) > \epsilon_0$, then $\phi_1 \to \sqrt{N}$ and $\phi_2 \to 0$, and all the energy will be localized on just one oscillator, hence the term "soliton."

IV. STABILITY ANALYSIS

To analyze the stability of stationary solutions, one needs to perturb the amplitude

$$\begin{aligned} i\frac{dA_n}{dt} &= V_n A_n - \gamma |A_n|^2 A_n - \epsilon_0(A_{n+1} + A_{n-1}) \\ &\quad - \epsilon_1 |A_{n+1}|^2 A_n, \\ A_1 &= \phi_1 + \delta_1(t), \end{aligned}$$

and

$$A_2 = \phi_2 + \delta_2(t).$$

We have added the perturbation $\delta(t)$ in a frame rotating with the stationary solution. $\delta_{1,2}$ are complex-valued and time-dependent. This leads to an evolution equation for the perturbations in the form of a (stability) matrix,

$$\frac{d}{dt}\begin{pmatrix}\mathrm{Re}(\delta(t))\\ \mathrm{Im}(\delta(t))\end{pmatrix} = \begin{pmatrix}0 & B\\ A & 0\end{pmatrix}\begin{pmatrix}\mathrm{Re}(\delta(t))\\ \mathrm{Im}(\delta(t))\end{pmatrix}, \tag{22}$$

where

$$A = \begin{pmatrix}\omega - V_1 + \gamma|\phi_1|^2 + \epsilon_1|\phi_2|^2 & \epsilon_0 \\ \epsilon_0 & \omega - V_2 + \gamma|\phi_2|^2 + \epsilon_1|\phi_1|^2\end{pmatrix} \tag{23}$$

and

$$B = \begin{pmatrix}V_1 - \omega - 3\gamma|\phi_1|^2 - \epsilon_1|\phi_2|^2 & -\epsilon_0 - 2\epsilon_1\phi_1\phi_2 \\ -\epsilon_0 - 2\epsilon_1\phi_1\phi_2 & V_2 - \omega - 3\gamma|\phi_2|^2 - \epsilon_1|\phi_1|^2\end{pmatrix}. \tag{24}$$

The eigenvalues of the stability matrix are computed by using

$$\det[AB - \lambda^2 I] = 0$$

and they are given as follows:

For the symmetric branch,

$$\lambda = 0$$

and

$$\lambda = -4\epsilon_0^2 - 2\epsilon_0\epsilon_1 N + 2\epsilon_0 N\gamma. \tag{25}$$

For the antisymmetric branch,

$$\lambda = 0$$

and

$$\lambda = -4\epsilon_0^2 + 2\epsilon_0\epsilon_1 N - 2\epsilon_0 N\gamma. \tag{26}$$

For the soliton branch,

$$\lambda_1 = \lambda_2 = -\epsilon_0^2. \tag{27}$$

The *symmetric solution* is stable for

$$0 < \gamma < \frac{2(V_1 - \omega - \epsilon_0)}{N} - \epsilon_1$$

and

$$0 < \epsilon_1 < \frac{2(V_2 - \omega - \epsilon_0)}{N} - \gamma.$$

The *antisymmetric solution* is stable for

$$\gamma > \frac{2(\epsilon_0 + V_1 - \omega)}{N} - \epsilon_1$$

and

$$0 < \epsilon_1 < \frac{2(\epsilon_0 + V_2 - \omega)}{N} - \gamma.$$

The *soliton solution* is stable for

$$\gamma > \frac{2(V_1 - \omega - \epsilon_0)}{N} - \epsilon_1,$$

$$\epsilon_1 > \frac{2(V_2 - \omega - \epsilon_0)}{N} - \gamma,$$

and

$$\epsilon_1 > \frac{2(\epsilon_0 + V_2 - \omega)}{N} - \gamma.$$

V. BIFURCATION DIAGRAMS

Figures 9, 11, 13, and 15 are the plots between γ and W $(= V_0 - \omega)$. Figures 10, 12, 14, and 16 are the plots between ϵ_1 and W. We have defined $V_1 = V_0(1 + \varepsilon)$ and $V_2 = V_0(1 - \varepsilon)$, as before. A similar stability analysis for exact stationary solutions was done in [26] for the purely cubic case. In these figures, the red line represents the antisymmetric $(\uparrow\downarrow)$ branch, green represents the symmetric $(\uparrow\uparrow)$ branch, and blue is the soliton $(\uparrow .)$ branch. The unstable solutions lie on the dashed lines. Increasing nonlocal (intersite) nonlinearity causes a shift in the bifurcation point, thereby reducing the effect of local (on-site) nonlinearity. This makes the symmetric solution more stable, but the antisymmetric solution is then stable only for $0 < \gamma < \frac{2(\epsilon_0+V_1-\omega)}{N} - \epsilon_1$. Increasing local nonlinearity also makes the solution more stable, but in this case the effect of nonlocal nonlinearity is reduced by a factor of $-\gamma$. In fact, one can see that an increase in at least one of the nonlinearity parameters (γ,ϵ_1) causes the bifurcation point to shift toward increasing stability. However, for fixed γ and ϵ_1, increasing asymmetry ε (even at very high strengths) does not have a

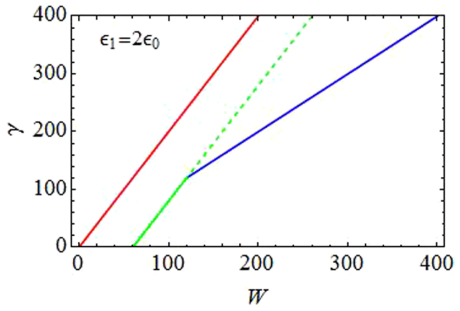

FIG. 9. Stationary solutions in the W-γ plane for $\varepsilon = 0.05$ with nonlocal response ϵ_1 twice as strong as the coupling ϵ_0 between adjacent sites: Extended DNLS dimer.

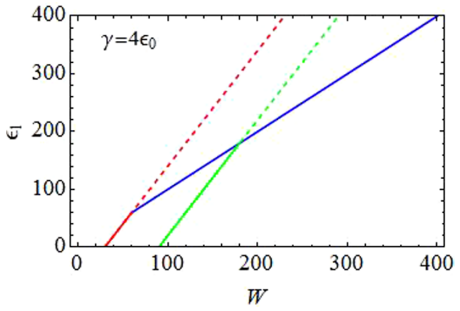

FIG. 10. Stationary solutions in the W-ϵ_1 plane for $\varepsilon = 0.05$ with local cubic response γ four times as strong as the coupling ϵ_0 between adjacent sites. Extended DNLS dimer.

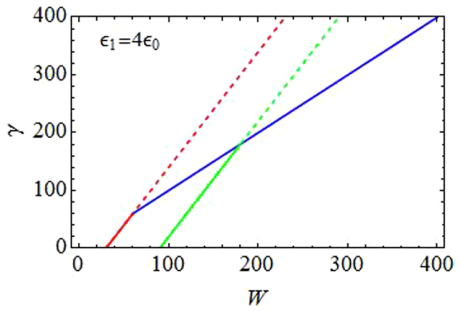

FIG. 11. Stationary solutions in the W-γ plane for $\varepsilon = 0.05$ and with $\epsilon_1 = 4\epsilon_0$. Extended DNLS dimer.

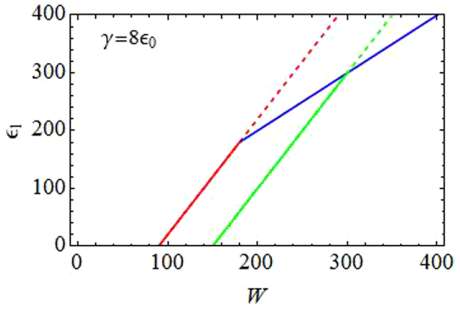

FIG. 12. Stationary solutions in the W-ϵ_1 plane for $\varepsilon = 0.05$ and with $\gamma = 8\epsilon_0$. Extended DNLS dimer.

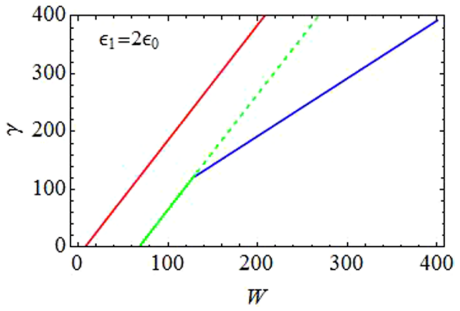

FIG. 13. Stationary solutions in the W-γ plane for $\varepsilon = 3$ and with $\epsilon_1 = 2\epsilon_0$. Extended DNLS dimer.

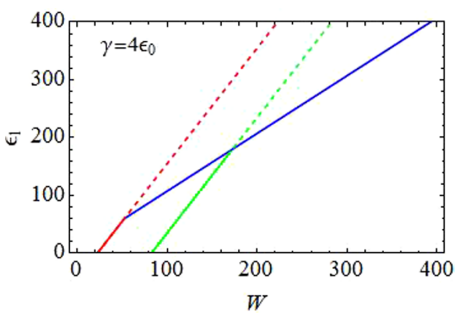

FIG. 14. Stationary solutions in the W-ϵ_1 plane for $\varepsilon = 3$ and with $\gamma = 4\epsilon_0$. Extended DNLS dimer.

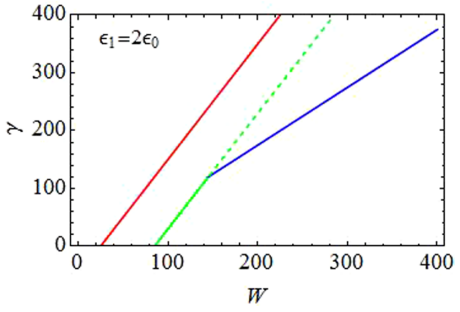

FIG. 15. Stationary solutions in the W-γ plane for $\varepsilon = 10$ and with $\epsilon_1 = 2\epsilon_0$. Extended DNLS dimer.

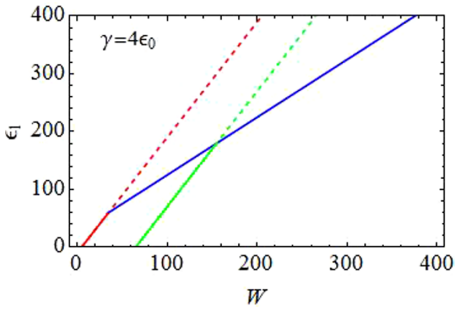

FIG. 16. Stationary solutions in the W-ϵ_1 plane for $\varepsilon = 10$ and with $\gamma = 4\epsilon_0$. Extended DNLS dimer.

significant effect on the shift of the bifurcation point, as can be seen in Figs. 13–16. Asymmetry ε is held fixed at $\varepsilon = 0.05$ for the first four plots (Figs. 9–12), is strengthened to $\varepsilon = 3$ for the plots in Figs. 13 and 14, and is further strengthened to $\varepsilon = 10$ for the plots in Figs. 15 and 16.

VI. SUMMARY AND CONCLUSION

We have discussed asymmetric propagation through an extended DNLS dimer. The important extension corresponds to a nonlocal (intersite) nonlinear response in addition to a purely cubic local (on-site) response. How this cooperative (local+nonlocal) nonlinearity embedded in the lattice effects the transmission of incoming waves and its effects on the diode action brought about by the nonreciprocal transmission is addressed. In short, we have presented a wave diode proposal for an extended DNLS dimer in view of earlier studies on the cubic DNLS model [18,19]. We assumed a lattice where the medium between the two nonlinear sites (dimer) is also nonlinear, which motivated the extension in the already existing proposal for the purely cubic DNLS model. We observed that the window of maximal transmission shrinks, as compared to the cubic case; however, maximal transmission takes place at lower input intensities. We also showed that this interval can be broadened by increasing the asymmetry in the on-site potentials, but the overall transmission is reduced with increasing asymmetry, as can be seen in Fig. 8, also noticed in [18] for the cubic case.

We obtained the transmission coefficients for a wave impinging the lattice from left and right. The rectifying factor is defined in order to determine the regions where diode action takes place and its efficiency in that region. We presented a series of plots by varying different site-dependent parameters to better understand the wave transmission phenomenon. Different plots for the transmission coefficients and rectifying factor were presented to signify the diode effect. We found that in the extended DNLS case, an almost perfect diode action takes place at a higher level of asymmetry ($\varepsilon = 0.7$) as compared to the cubic DNLS case ($\varepsilon = 0.4$). Moreover, there is a higher contribution from left-moving waves for a perfect diode action as compared to right-moving waves. This trend is exactly the opposite in the purely cubic case. The transmission pattern is also found to be symmetric between incoming waves with larger and smaller wave numbers.

We also investigated the stability of exact stationary solutions to this extended (asymmetric) DNLS dimer, and we plotted the corresponding bifurcation diagrams to analyze the bifurcation behavior. We noticed that the inclusion of the nonlocal (intersite) nonlinearity reduces the effect of local (cubic) nonlinearity, which effects the bifurcation behavior, i.e., increasing the strength of the nonlocal nonlinearity shifts the bifurcation point thus rendering the corresponding solution branch more stable and hence dominating the effect of local nonlinearity.

It will be interesting to study the corresponding case when one saturates this cooperative nonlinear response. This can allow an even finer tuning for the diode action because of the presence of an extra system parameter, "saturation." The work in this direction is in progress, and we hope to report our results soon.

ACKNOWLEDGMENTS

M.A.W. would like to gratefully acknowledge extensive help from Magnus Johansson. Helpful discussions with Meng Sun, Sergej Flach, and Hee Chul Park are also acknowledged. M.A.W. would also like to thank the IBS Center for Theoretical Physics of Complex Systems in Daejeon, South Korea, where a major part of this work was carried out, for hospitality and financial support.

[1] X. F. Li, X. Ni, L. A. Feng, M. H. Lu, C. He, and Y. F. Chen, Phys. Rev. Lett. **106**, 084301 (2011).
[2] N. Boechler, G. Theocharis, and C. Daraio, Nat. Mater. **10**, 665 (2011).
[3] B. Yuan, B. Liang, J. C. Tao, X. Y. Zou, and J. C. Cheng, Appl. Phys. Lett. **101**, 043503 (2012).
[4] C. W. Chang, D. Okawa, A. Majumdar, and A. Zettl, Science **314**, 1121 (2006).
[5] T. Sun, J. X. Wang, and W. Kang, Europhys. Lett. **105**, 16004 (2014).
[6] Y. Wang, A. Vallabhaneni, J. N. Hu, B. Qiu, Y. P. Chen, and X. L. Ruan, Nano Lett. **14**, 592 (2014).
[7] K. Gallo, G. Assanto, K. R. Parameswaran, and M. M. Fejer, Appl. Phys. Lett. **79**, 314 (2001).
[8] L. Fan, J. Wang, L. T. Varghese, H. Shen, B. Niu, Y. Xuan, A. M. Weiner, and M. H. Qi, Science **335**, 447 (2012).
[9] D. Roy, Phys. Rev. B **81**, 155117 (2010).
[10] H. Lira, Z. F. Yu, S. H. Fan, and M. Lipson, Phys. Rev. Lett. **109**, 033901 (2012).
[11] J. Rayleigh, *The Theory of Sound* (Dover, New York, 1945).
[12] A. Figotin and I. Vitebsky, Phys. Rev. E **63**, 066609 (2001).
[13] A. B. Khanikaev and M. J. Steel, Opt. Express **17**, 5265 (2009).
[14] R. Fleury *et al.*, Science **343**, 516 (2014).
[15] Yu. A. Kosevich, Phys. Rev. B **52**, 1017 (1995).
[16] M. Scalora, J. P. Dowling, C. M. Bowden, and M. J. Bloemer, J. Appl. Phys. **76**,2023 (1994).
[17] M. D. Tocci, M. J. Bloemer, M. Scalora, J. P. Dowling, and C. M. Bowden, Appl. Phys. Lett. **66**, 2324 (1995).
[18] S. Lepri and G. Casati, Phys. Rev Lett. **106**, 164101 (2011).
[19] S. Lepri and G. Casati, *Localized Excitations in Nonlinear Complex Systems: Current State of the Art and Future Perspectives*, Nonlinear Systems and Complexity, Vol. 7 (Springer, Cham, Switzerland, 2014).
[20] E. Johansson, Diploma thesis, Linköping University, http://urn:nbn:se:liu:diva-111236.
[21] T. F. Assunção, E. M. Nascimento, and M. L. Lyra, Phys. Rev. E **90**, 022901 (2014).
[22] J. D'Ambroise, P. G. Kevrekidis, and S. Lepri, J. Phys. A **45**, 444012 (2012).

[23] H. S. Eisenberg, Y. Silberberg, R. Morandotti, A. R. Boyd, and J. S. Aitchison, Phys. Rev. Lett. **81**, 3383 (1998).
[24] C. Falvo, V. Pouthier, and J. C. Eilbeck, Physica D **221**, 58 (2006).
[25] V. Pouthier, Physica D **221**, 13 (2006).
[26] J. Carr and J. C. Eilbeck, Phys. Lett. A **109**, 201 (1985).
[27] B. Lindquist, Phys. Rev. E **63**, 056605 (2001).
[28] G. Tsironis and D. Hennig, Phys. Rep. **307**, 333 (1999).
[29] F. Delyon, Y.-E. Lévy, and B. Souillard, Phys. Rev. Lett. **57**, 2010 (1986).
[30] Q. Li, C. T. Chan, K. M. Ho, and C. M. Soukoulis, Phys. Rev. B **53**, 15577 (1996).